Proceedings of the ASME 2013 International Mechanical Engineering Congress and Exposition
IMECE2013
November 15-21, 2013, San Diego, California, USA

IMECE2013-64694

DESIGNING PHONONIC CRYSTALS WITH CONVEX OPTIMIZATION

Han Men*
Department of Aeronautics and Astronautics
Massachusetts Institute of Technology
Cambridge, MA 02139
Email: abbymen@mit.edu

Robert. M. Freund
Sloan School of Management
Ngoc C. Nguyen, Joel Saa-Seoane, Jaime Peraire
Department of Aeronautics and Astronautics
Massachusetts Institute of Technology
Cambridge, MA 02139

ABSTRACT

Designing phononic crystals by creating frequency bandgaps is of particular interest in the engineering of elastic and acoustic microstructured materials. Mathematically, the problem of optimizing the frequency bandgaps is often nonconvex, as it requires the maximization of the higher indexed eigenfrequency and the minimization of the lower indexed eigenfrequency. A novel algorithm [1] has been previously developed to reformulate the original nonlinear, nonconvex optimization problem to an iteration-specific semidefinite program (SDP). This algorithm separates two consecutive eigenvalues – effectively maximizing bandgap (or bandwidth) – by separating the gap between two orthogonal subspaces, which are comprised columnwise of "important" eigenvectors associated with the eigenvalues being bounded. By doing so, we avoid the need of computation of eigenvalue gradient by computing the gradient of affine matrices with respect to the decision variables. In this work, we propose an even more efficient algorithm based on linear programming (LP). The new formulation is obtained via approximation of the semidefinite cones by judiciously chosen linear bases, coupled with "delayed constraint generation". We apply the two convex conic formulations, namely, the semidefinite program and the linear program, to solve the bandgap optimization problems. By comparing the two methods, we demonstrate the efficacy and efficiency of the LP-based algorithm in solving the category of eigenvalue bandgap optimization problems.

*Address all correspondence to this author.

1 INTRODUCTION

Phononic crystal, as an elastic and acoustic analogue of the photonic crystal, is a periodic microstructure created from the arrangement of composite elastic materials. Similar to the frequency bandgap to electromagnetic wave propagation in photonic crystals, it is also possible for phononic crystals to exhibit a range of prohibitive frequencies in their transmission spectra to the propagation of elastic and/or acoustic waves of any polarization or wave vector. This property lends phononic bandgap structures to a wide range of applications – acoustic mirrors, filters, and waveguides. Among many important studies on phononic crystals, the design of phononic crystals with optimal bandgaps is undoubtedly still the most fundamental topic, as it provides the building block for other extensive applications [2, 3, 4].

The design problem of the basic periodic structure of phononic crystals can be mathematically formulated as an infinite-dimensional, nonlinear, nonconvex optimization problem in very much the same way as the bandgap optimization problem for photonic crystals: find a periodic configuration of the prescribed composite materials that is parameterized by a spatial function $\sigma(\boldsymbol{r})$, such that the designated frequency gap between two consecutive frequency bands (often expressed as a fractional function in terms of two consecutive eigenvalues) is optimized [5].

Wheather the considered structure is infinite bulk material [6] or moderately thick plates [7, 8], Bloch theory can be employed to reduce the computation domain to a single primitive cell of the periodic lattice. Among various strategies for geometry representation of the computational design domain(e.g.,

topology optimization and shape optimization), the method of topology optimization has convincingly established its superiority as it provides the most flexible and effective conceptual design proposals [9]. In topology optimization, the unknown $\sigma(\boldsymbol{r})$ is discretized into an array of binary variables (or linear bounded variables in the relaxed setting), and each variable represents the material property at a grid point or a piecewise constant/linear element of the computation domain. The analysis part of the problem involves solving the governing eigenvalue equation with numerical schemes such as finite element method [10], and the design part of the problem seeks the optimial solution of the discrete geometry/material variables. To obtain the solution of these discrete variables to a nonlinear and nonconvex optimization problem using mathematical programming, gradient based nonlinear solvers are often used for convenience (e.g., Method of Moving Asymptote [11]). In our earlier works [1, 12], a linear and convex algorithm was proposed instead. This algorithm makes use of subspace approximation to reformulate the original problem as a sequence of convex semidefinite programs (SDPs), and hence can be efficiently solved by interior point methods. Another advantage of the SDP formulation is that it avoids the calculation of the eigenvalue gradients required in other methods (such as the MMA based works [5, 13]), which can be problematic in case of eigenvalue multiplicity or high density of states.

While topology optimization has proven reliable in the concept level of the design process, the optimal design proposals obtained are often not guaranteed to be feasible for direct fabrication, either due to (i) the deliberate simplification of a model, (ii) technological limitations, and/or (iii) human factors. To overcome these challenges, we developed a new modeling paradigm called "fabrication-adaptive optimization" [14] that stems from the robust regularization of a function [15]. Unfortunately, the fabrication adaptive counterpart of a SDP problem is NP-hard, which motivates us to instead work with an LP relaxation of the SDP problem. The new LP formulation is obtained via approximation of the semidefinite cones by judiciously chosen linear bases and coupled with "delayed constraint generation". Although being a somewhat heuristic method, the LP relaxation has shown improved performance compared to the SDP formulation when solving the bandgap optimization problems for photonic crystals.

In this paper, we extend the study of the LP formulation to additional design problems of microstructured materials, such as phononic bandgap structures. We first introduce the phononic crystal bandgap optimization problem in section 2, and briefly review the SDP algorithm in section 3 for completeness. The formulation based on linear programming is discussed in details in section 4. In section 5, we compare the performance of the SDP and LP formulations, and present the optimal phononic bandgap structures of different propagation modes and different lattice structures. The concluding remarks are presented in section 6.

2 PROBLEM STATEMENT

Elastic wave propagation in a continuous media is governed by the following equations of motion,

$$\rho\ddot{u}_i = \frac{\partial}{\partial x_i}(\lambda\nabla\cdot\boldsymbol{u}) + \nabla\cdot(\mu\nabla u_i + \mu\frac{\partial \boldsymbol{u}}{\partial x_i}) + f_i,\ i=1,2,3,\ \text{in}\ \mathbb{R}^3. \tag{1}$$

The equation describes the displacement $\boldsymbol{u} = (u_1, u_2, u_3)$ and acceleration $\ddot{\boldsymbol{u}}$ of a small elemental volume with density ρ when it is subject to external body force $\boldsymbol{f} = (f_1, f_2, f_3)$ and internal strain. The constants λ and μ are known as the Lamé parameters. These constants can also be expressed in terms of other familiar elastic parameters such as Young's modulus E and Poisson's ratio σ: $\lambda = \frac{E}{(1+\sigma)(1-2\sigma)}$, $\mu = \frac{E}{2(1+\sigma)}$.

A phononic crystal is a periodic lattice-like structure with primitive lattice vectors $\boldsymbol{a}_1 = a_1\hat{\boldsymbol{e}}_1$, $\boldsymbol{a}_2 = a_2\hat{\boldsymbol{e}}_2$, and $\boldsymbol{a}_3 = a_3\hat{\boldsymbol{e}}_3$. For every lattice vector $\boldsymbol{R}$ written in terms of the primitive lattice vectors, i.e., $\boldsymbol{R} = m_1\boldsymbol{a}_1 + m_2\boldsymbol{a}_2 + m_3\boldsymbol{a}_3$, and any spatial coordinate $\boldsymbol{r} = x_1\hat{\boldsymbol{e}}_1 + x_2\hat{\boldsymbol{e}}_2 + x_3\hat{\boldsymbol{e}}_3$, the material properties in a phononic crystal satisfy the periodic condition, $\rho(\boldsymbol{r}) = \rho(\boldsymbol{r}+\boldsymbol{R})$, $\lambda(\boldsymbol{r}) = \lambda(\boldsymbol{r}+\boldsymbol{R})$, and $\mu(\boldsymbol{r}) = \mu(\boldsymbol{r}+\boldsymbol{R})$.

We consider only the elastic structures with two-dimensional periodicity and no body force ($\boldsymbol{f} = 0$) in this work. Two-dimensional periodicity means that the material only varies periodically in, say, the $\hat{\boldsymbol{e}}_1$–$\hat{\boldsymbol{e}}_2$ plane, and is invariant in the $\hat{\boldsymbol{e}}_3$ direction, i.e., $a_3 = 0$. This implies that the displacement field should also be independent of x_3, i.e., $\boldsymbol{u}(x_1, x_2, x_3) = \boldsymbol{u}(x_1, x_2)$, or $\partial\boldsymbol{u}/\partial x_3 = 0$. We can rewrite equation (1) as

$$\rho\ddot{u}_1 = \frac{\partial}{\partial x_1}\Big[(\lambda+2\mu)\frac{\partial u_1}{\partial x_1} + \lambda\frac{\partial u_2}{\partial x_2}\Big] + \frac{\partial}{\partial x_2}\Big(\mu\frac{\partial u_1}{\partial x_2} + \mu\frac{\partial u_2}{\partial x_1}\Big), \tag{2a}$$

$$\rho\ddot{u}_2 = \frac{\partial}{\partial x_1}\Big(\mu\frac{\partial u_2}{\partial x_1} + \mu\frac{\partial u_1}{\partial x_2}\Big) + \frac{\partial}{\partial x_2}\Big[(\lambda+2\mu)\frac{\partial u_2}{\partial x_2} + \lambda\frac{\partial u_1}{\partial x_1}\Big], \tag{2b}$$

$$\rho\ddot{u}_3 = \frac{\partial}{\partial x_1}\Big(\mu\frac{\partial u_3}{\partial x_1}\Big) + \frac{\partial}{\partial x_2}\Big(\mu\frac{\partial u_3}{\partial x_2}\Big). \tag{2c}$$

Applying the Bloch theorem for wave propagation in the periodic medium, the displacement of the movement can be represented as

$$\boldsymbol{u} = \tilde{\boldsymbol{u}}e^{i(\boldsymbol{k}\cdot\boldsymbol{r}+\omega t)}, \tag{3}$$

where $\boldsymbol{k} = (k_1, k_2, k_3)$ is the wavevector, and ω is the wave frequency. The displacement $\tilde{\boldsymbol{u}}$ is an envelope function that is periodic in $\mathbb{R}^3$, i.e., $\tilde{\boldsymbol{u}}(\boldsymbol{r}) = \tilde{\boldsymbol{u}}(\boldsymbol{r}+\boldsymbol{R})$. The computation can thus be reduced to one primitive cell of the phononic crystal, $\Omega \subset \mathbb{R}^2$.

Substituting (3) into (2) and simplifying, we obtain the first equation,

$$\begin{aligned}-\omega^2\rho\tilde{u}_1 &= \frac{\partial}{\partial x_1}\Big[(\lambda+2\mu)\frac{\partial\tilde{u}_1}{\partial x_1}\Big] - k_1^2(\lambda+2\mu)\tilde{u}_1 \\ &+ ik_1(\lambda+2\mu)\frac{\partial\tilde{u}_1}{\partial x_1} + ik_1\frac{\partial}{\partial x_1}\big[(\lambda+2\mu)\tilde{u}_1\big] \\ &+ \frac{\partial}{\partial x_2}\Big(\mu\frac{\partial\tilde{u}_1}{\partial x_2}\Big) + ik_2\mu\frac{\partial\tilde{u}_1}{\partial x_2} + ik_2\frac{\partial}{\partial x_2}(\mu\tilde{u}_1) - k_2^2\mu\tilde{u}_1 \\ &+ \frac{\partial}{\partial x_1}\Big(\lambda\frac{\partial\tilde{u}_2}{\partial x_2}\Big) + ik_1\lambda\frac{\partial\tilde{u}_2}{\partial x_2} + ik_2\frac{\partial}{\partial x_1}(\lambda\tilde{u}_2) - k_1k_2\lambda\tilde{u}_2 \\ &+ \frac{\partial}{\partial x_2}\Big(\mu\frac{\partial\tilde{u}_2}{\partial x_1}\Big) + ik_2\mu\frac{\partial\tilde{u}_2}{\partial x_1} + ik_1\frac{\partial}{\partial x_2}(\mu\tilde{u}_2) - k_1k_2\mu\tilde{u}_2,\end{aligned} \tag{4a}$$

the second equation,

$$\begin{aligned}-\omega^2\rho\tilde{u}_2 &= \frac{\partial}{\partial x_1}\Big(\mu\frac{\partial\tilde{u}_2}{\partial x_1}\Big) + ik_1\mu\frac{\partial\tilde{u}_2}{\partial x_1} + ik_1\frac{\partial}{\partial x_1}(\mu\tilde{u}_2) - k_1^2\mu\tilde{u}_2 \\ &+ \frac{\partial}{\partial x_2}\Big[(\lambda+2\mu)\frac{\partial u_2}{\partial x_2}\Big] - k_2^2(\lambda+2\mu)\tilde{u}_2 \\ &+ ik_2(\lambda+2\mu)\frac{\partial\tilde{u}_2}{\partial x_2} + ik_2\frac{\partial}{\partial x_2}[(\lambda+2\mu)\tilde{u}_2] \\ &+ \frac{\partial}{\partial x_1}\Big(\mu\frac{\partial\tilde{u}_1}{\partial x_2}\Big) + ik_1\mu\frac{\partial\tilde{u}_1}{\partial x_2} + ik_2\frac{\partial}{\partial x_1}(\mu\tilde{u}_1) - k_1k_2\mu\tilde{u}_1 \\ &+ \frac{\partial}{\partial x_2}\Big(\lambda\frac{\partial\tilde{u}_1}{\partial x_1}\Big) + ik_2\lambda\frac{\partial\tilde{u}_1}{\partial x_1} + ik_1\frac{\partial}{\partial x_2}(\lambda\tilde{u}_1) - k_1k_2\lambda\tilde{u}_1,\end{aligned} \tag{4b}$$

and the third equation,

$$\begin{aligned}-\omega^2\rho\tilde{u}_3 &= \frac{\partial}{\partial x_1}\Big(\mu\frac{\partial\tilde{u}_3}{\partial x_1}\Big) + ik_1\mu\frac{\partial\tilde{u}_3}{\partial x_1} + ik_1\frac{\partial}{\partial x_1}(\mu\tilde{u}_3) - k_1^2\mu\tilde{u}_3 \\ &+ \frac{\partial}{\partial x_2}\Big(\mu\frac{\partial\tilde{u}_3}{\partial x_2}\Big) + ik_2\mu\frac{\partial\tilde{u}_3}{\partial x_2} + ik_2\frac{\partial}{\partial x_2}(\mu\tilde{u}_3) - k_2^2\mu\tilde{u}_3.\end{aligned} \tag{4c}$$

We can see that $\tilde{u}_1$ and $\tilde{u}_2$ are coupled through (4a) and (4b), while $\tilde{u}_3$ is independently governed by (4c). In the literature of elastic wave propagation and phononic crystals [16, 5], the decoupling of $\tilde{u}_3$ from the other two displacement components is often treated as *out-of-plane* propagation, while the coupling of $\tilde{u}_1$ and $\tilde{u}_2$ is known as *in-plane* propagation. These two propagation modes can exist independently (analogous to the transverse-electric (TE) or transverse-magnetic (TM) mode of the electromagnetic wave propagation in photonic crystals) or simultaneously (analogous to the combined TEM mode in photonic crystals). Regardless of the propagation mode being discussed, all can be analyzed in a unified way by studying the discrete governing equation of analogous format. Next, we employ a similar discretization strategy as proposed in the design of photonic crystals.

First, to completely characterize the dispersion relation $\omega(\boldsymbol{k})$ of the periodic structure, it is customary to trace the boundary of the irreducible Brillouin zone (denoted by $\partial\mathscr{B}$) where the optima of $\omega(\boldsymbol{k})$ occur, and consider only a finite number $n_{\boldsymbol{k}}$ of wave vectors in the set

$$\mathscr{P} \equiv \{\boldsymbol{k}_t \in \partial B,\ 1 \le t \le n_k\}. \tag{5}$$

Second, we assume the phononic crystal is made up of two homogenous phases of materials, and the mechanical properties of the two prescribed materials are ρ_L, λ_L, μ_L, and ρ_H, λ_H, μ_H, respectively. Next we use a distribution function $\sigma(\boldsymbol{r}) = \sigma(x_1, x_2) \in [0,1]$ to represent the proportion of the two materials. The computation domain Ω is then discretized into N_t elements on which $\sigma(\boldsymbol{r})$ takes piecewise-constant values between 0 and 1. The discretized distribution function $\sigma(\boldsymbol{r})$ is denoted by a vector $\boldsymbol{\sigma}$ whose components represent the material property of each element of the unit cell:

$$\mathscr{Q} \equiv \{\boldsymbol{\sigma} : \boldsymbol{\sigma} = (\sigma_1, \sigma_2, \ldots, \sigma_{n_\sigma})^T \in [0,1]^{n_\sigma}\}. \tag{6}$$

The symmetry of the prescribed lattice is also taken into consideration to reduce the number of discrete variables necessary to represent the structure, hence $n_\sigma < N_t$. To approximate the discrete mechanical properties of the composite material, $\boldsymbol{\rho} = (\rho_1, \ldots, \rho_{n_\sigma})^T$, $\boldsymbol{\lambda} = (\lambda_1, \ldots, \lambda_{n_\sigma})^T$, and $\boldsymbol{\mu} = (\mu_1, \ldots, \mu_{n_\sigma})^T$, linear interpolation of the two prescribed phases is used,

$$\begin{aligned}\rho_i &= \sigma\rho_H + (1-\sigma_i)\rho_L = \sigma_i(\rho_H - \rho_L) + \rho_L, \\ \lambda_i &= \sigma\lambda_H + (1-\sigma_i)\lambda_L = \sigma_i(\lambda_H - \lambda_L) + \lambda_L, \\ \mu_i &= \sigma\mu_H + (1-\sigma_i)\mu_L = \sigma_i(\mu_H - \mu_L) + \mu_L.\end{aligned} \tag{7}$$

Third, we use a Galerkin finite element method with piecewise linear polynomials to approximate the system in (4), and derive the following discrete eigenvalue problem:

$$\mathscr{A}(\boldsymbol{\sigma}, \boldsymbol{k})u_j = \chi_j\mathscr{M}(\boldsymbol{\sigma})u_j,\ \ \boldsymbol{\sigma} \in \mathscr{Q},\ \boldsymbol{k} \in \mathscr{P},\ j = 1, 2, \ldots, \mathscr{N}. \tag{8}$$

Equation (8) could represent either the in-plane propagation mode in equations (4a) and (4b) where $u_j := (\tilde{u}_1, \tilde{u}_2)_j^T$, or

the out-of-plane propagation mode in (4c) where $u_j := (\tilde{u}_3)_j$, or both propagation modes with all three equations in (4) where $u_j := (\tilde{u}_1, \tilde{u}_2, \tilde{u}_3)_j^T$. The Hermitian stiffness matrix $\mathscr{A}(\boldsymbol{\sigma}, \boldsymbol{k}) \in \mathbb{C}^{\mathscr{N}\times\mathscr{N}}$ and the symmetric positive definite mass matrix $\mathscr{M}(\boldsymbol{\sigma}) \in \mathbb{R}^{\mathscr{N}\times\mathscr{N}}$ for all three problems follow the same affine σ-dependence,

$$\mathscr{A}(\boldsymbol{\sigma}, \boldsymbol{k}) = \mathscr{A}_0(\boldsymbol{k}) + \sum_{i=1}^{n_\sigma} \sigma_i \mathscr{A}_i(\boldsymbol{k}),\ \mathscr{M}(\boldsymbol{\sigma}) = \mathscr{M}_0 + \sum_{i=1}^{n_\sigma} \sigma_i \mathscr{M}_i. \tag{9}$$

In the following, we will use superscripts $(\cdot)^{IP}$, $(\cdot)^{OP}$, and $(\cdot)^{IOP}$ on the respective matrices to specify each of these three propagations. By convention, matrices without superscripts indicate a general formulation that applies to all three cases.

The central and the most fundamental problem of phononic crystal design is to identify a configuration of crystal structure, or $\boldsymbol{\sigma}$, such that one or multiple selected *eigenvalue gap-midgap* ratios is(are) maximized. Let $\mathscr{J} = \{m_j | 1 \le j \le J\}$ denote a set of J bands for which we seek to achieve gaps. The jth bandgap is defined as the *eigenvalue gap-midgap ratio* between bands m_j and $m_j + 1$, and is denoted as:

$$R^j(\boldsymbol{\sigma}) = \frac{\min\limits_{\boldsymbol{k}\in\mathscr{P}} \chi_{m_j+1}(\boldsymbol{\sigma}, \boldsymbol{k}) - \max\limits_{\boldsymbol{k}\in\mathscr{P}} \chi_{m_j}(\boldsymbol{\sigma}, \boldsymbol{k})}{\frac{1}{2}\left(\min\limits_{\boldsymbol{k}\in\mathscr{P}} \chi_{m_j+1}(\boldsymbol{\sigma}, \boldsymbol{k}) + \max\limits_{\boldsymbol{k}\in\mathscr{P}} \chi_{m_j}(\boldsymbol{\sigma}, \boldsymbol{k})\right)}. \tag{10}$$

The optimization problem to be solved is then:

$$\begin{aligned} \max_{\boldsymbol{\sigma}\in\mathscr{Q}}\ \min_{1\le j\le J}\ & \alpha_j R^j(\boldsymbol{\sigma}) \\ \text{s.t. } & \mathscr{A}(\boldsymbol{\sigma}, \boldsymbol{k}) u_{m_j} = \chi_{m_j} \mathscr{M}(\boldsymbol{\sigma}) u_{m_j}, \\ & \mathscr{A}(\boldsymbol{\sigma}, \boldsymbol{k}) u_{m_j+1} = \chi_{m_j+1} \mathscr{M}(\boldsymbol{\sigma}) u_{m_j+1}, \\ & \text{for } j = 1, \ldots, J,\ \boldsymbol{k} \in \mathscr{P}. \end{aligned} \tag{11}$$

The $\alpha_j, j = 1, \ldots, J$, are prescribed weights for each bandgap. By adjusting α_j, one can obtain optimal crystal structures with varying emphasis among the multiple bandgaps, see [12] for such a trade-off study in the context of photonic crystal design. In otherwise general computations we typically set $\alpha_j = 1,\ j = 1 \ldots, J$.

3 SDP RELAXATION

Problem (11) is clearly nonlinear and nonconvex. In our previous work [1, 12] on the optimal design of photonic crystal bandgap structures, an algorithm has been sucessfully developed to relax such an optimization problem to an iteration-specific semidefinite program (SDP). The same approach can be applied to problem (11). A short review of the SDP problem is provided here for completeness.

Let $\hat{\boldsymbol{\sigma}}$ be the current iterate. We construct two subspace matrices for each of the target bandgaps at each $\boldsymbol{k} \in \mathscr{P}$. For each $\boldsymbol{k} \in \mathscr{P}$, we have,

$$\Phi_j^{\hat{\boldsymbol{\sigma}},\ell}(\boldsymbol{k}) = [u_{m_j - N_{j\boldsymbol{k}}^\ell + 1}(\hat{\boldsymbol{\sigma}}, \boldsymbol{k}), \ldots, u_{m_j}(\hat{\boldsymbol{\sigma}}, \boldsymbol{k})],$$

$$\Phi_j^{\hat{\boldsymbol{\sigma}},u}(\boldsymbol{k}) = [u_{m_j+1}(\hat{\boldsymbol{\sigma}}, \boldsymbol{k}), \ldots, u_{m_j+N_{j\boldsymbol{k}}^u}(\hat{\boldsymbol{\sigma}}, \boldsymbol{k})],$$

where $u_i(\hat{\boldsymbol{\sigma}}, \boldsymbol{k})$ are the orthonormal eigenvectors of the Hermitian eigenvalue equation (8) with $\boldsymbol{\sigma} = \hat{\boldsymbol{\sigma}}$. The dimensions of the subspace matrices are $\Phi_j^{\hat{\boldsymbol{\sigma}},\ell}(\boldsymbol{k}) \in \mathbb{C}^{\mathscr{N}\times N_{j\boldsymbol{k}}^\ell}$, $\Phi_j^{\hat{\boldsymbol{\sigma}},u}(\boldsymbol{k}) \in \mathbb{C}^{\mathscr{N}\times N_{j\boldsymbol{k}}^u}$. Ideally, $\Phi_j^{\hat{\boldsymbol{\sigma}},\ell}(\boldsymbol{k})$ and $\Phi_j^{\hat{\boldsymbol{\sigma}},u}(\boldsymbol{k})$ should include all the lower m_j eigenvectors, and all the higher $\mathscr{N} - m_j$ eigenvectors respectively. As proposed in [1], we instead work with a small "important" subset of these eigenvectors to reduce computation, i.e, $N_{j\boldsymbol{k}}^\ell \le m_j$, and $N_{j\boldsymbol{k}}^u \ll \mathscr{N} - m_j$. Typically, the dimensions of the subspaces are $3 - 7$. Readers are referred to the previous work for details on the construction of these reduced subspaces. Now the problem in (11) can be locally reformulated as follows,

$$\begin{aligned} \max_{\boldsymbol{\sigma},\ \boldsymbol{\chi}^\ell,\boldsymbol{\chi}^u,\ F}\ & F \\ \text{s.t.}\ & \Phi_j^{\hat{\boldsymbol{\sigma}},\ell *}(\boldsymbol{k}) \left[\mathscr{A}(\boldsymbol{\sigma}, \boldsymbol{k}) - \chi_j^\ell \mathscr{M}(\boldsymbol{\sigma})\right] \Phi_j^{\hat{\boldsymbol{\sigma}},\ell}(\boldsymbol{k}) \preceq 0, \\ & \Phi_j^{\hat{\boldsymbol{\sigma}},u *}(\boldsymbol{k}) \left[\mathscr{A}(\boldsymbol{\sigma}, \boldsymbol{k}) - \chi_j^u \mathscr{M}(\boldsymbol{\sigma})\right] \Phi_j^{\hat{\boldsymbol{\sigma}},u}(\boldsymbol{k}) \succeq 0, \\ & 2\alpha_j(\chi_j^u - \chi_j^\ell) - F(\chi_j^u + \chi_j^\ell) \ge 0, \\ & \chi_j^\ell, \chi_j^u, F \ge 0, \text{ for } j = 1, \ldots, J,\ \boldsymbol{k} \in \mathscr{P}, \end{aligned} \tag{12}$$

where "$\succeq$" is the Löwner partial ordering on symmetric matrices, i.e., $A \succeq B$ if and only if $A - B$ is positive semidefinite. As a result of the affinity of the stiffness and mass matrices (9), the constraints in the third row of (12) are bilinear, and can be linearized around the previous solution to obtain a linear semidefinite program. Note that if only one bandgap is to be optimized, i.e., J = 1, the third constraint row can be represented as a linear fractional objective function, and can be converted to a linear objective using standard homogenization [17]. The final formulation can be efficiently solved by modern SDP solvers, for example, the interior-point method based optimization solver SDPT3 [18].

4 LP RELAXATION

4.1 Approximation of the Eigenvalue Bounds using Linear Inequalities

We start from the definition of positive semi-definiteness of a matrix: an $N_{sp} \times N_{sp}$ matrix B is positive semi-definite if and only if $v^T B v \ge 0$ for all non-zero vectors v. That is to say, a linear

matrix inequality (LMI) of the form $B(x) := B_0 + \sum_{i=1}^{n} B_i x_i \succeq 0$ is equivalent to

$$b^T B(x) b \geq 0 \quad \forall b \in \mathbb{R}^{N_{sp}}. \tag{13}$$

We then approximate the above inequality by judiciously generating a finite number of approximating vectors $b^{(1)}, \ldots, b^{(N_B)} \in \mathbb{R}^{N_{sp}}$. (The method for choosing and updating these sets of vectors will be discussed in the next subsection.) We can multiply the two linearized SDP inclusions in (12) with appropriate approximating vectors, and reformatting by rescaling, we obtain the following two linear inequality systems:

$$B_j^{\hat{\boldsymbol{\sigma}},\ell}\boldsymbol{\sigma} + g_j^{\hat{\boldsymbol{\sigma}},\ell} \leq e\boldsymbol{\chi}_j^{\ell}, \qquad B_j^{\hat{\boldsymbol{\sigma}},u}\boldsymbol{\sigma} + g_j^{\hat{\boldsymbol{\sigma}},u} \geq e\boldsymbol{\chi}_j^{u}, \ j = 1, \ldots, J, \tag{14}$$

where $B_j^{\hat{\boldsymbol{\sigma}},\ell} \in \mathbb{C}^{(N_j^{\ell} n_k) \times n_\sigma}$, $g_j^{\hat{\boldsymbol{\sigma}},\ell} \in \mathbb{C}^{N_j^{\ell} n_k}$, $B_j^{\hat{\boldsymbol{\sigma}},u} \in \mathbb{C}^{(N_j^{u} n_k) \times n_\sigma}$, and $g_j^{\hat{\boldsymbol{\sigma}},u} \in \mathbb{C}^{N_j^{u} n_k}$. These two families of inequalities are concatenation of the sets of linear inequalities for each of the $\boldsymbol{k}$ points, i.e., $N_j^{\ell} = \sum_{\boldsymbol{k} \in \mathscr{P}} N_{j\boldsymbol{k}}^{\ell}$, and $N_j^{u} = \sum_{\boldsymbol{k} \in \mathscr{P}} N_{j\boldsymbol{k}}^{u}$. Replacing the semidefinite inclusions in (12) with their linear inequality approximations (14), we obtain the following almost linear approximation of (12):

$$\begin{aligned} P_{LP}^{\hat{\boldsymbol{\sigma}}}: \ \max_{\boldsymbol{\sigma},\, \boldsymbol{\chi}^{\ell},\, \boldsymbol{\chi}^{u},\, F} \quad & F \\ \text{s.t.} \quad & B_j^{\hat{\boldsymbol{\sigma}},\ell}\boldsymbol{\sigma} + g_j^{\hat{\boldsymbol{\sigma}},\ell} \leq e\boldsymbol{\chi}_j^{\ell}, \\ & B_j^{\hat{\boldsymbol{\sigma}},u}\boldsymbol{\sigma} + g_j^{\hat{\boldsymbol{\sigma}},u} \geq e\boldsymbol{\chi}_j^{u}, \\ & 2\alpha_j(\chi_j^{u} - \chi_j^{\ell}) - F(\chi_j^{u} + \chi_j^{\ell}) \geq 0, \\ & \chi_j^{\ell}, \chi_j^{u}, F \geq 0, \text{ for } j = 1, \ldots, J, \ \ \boldsymbol{k} \in \mathscr{P}. \end{aligned} \tag{15}$$

where $e = (1, \ldots, 1)$ denotes the vector of ones, whose dimension will be given in context. The third constraint is bilinear and can be linearized as before. In order for the LP formulation to be reasonably accurate, the optimal solution $\boldsymbol{\sigma}^*$ of (15) should be close enough to the linearizing point $\hat{\boldsymbol{\sigma}}$, i.e., $\|\boldsymbol{\sigma}^* - \hat{\boldsymbol{\sigma}}\| \leq \varepsilon_{\text{tol}}$. Problem $P_{LP}^{\hat{\boldsymbol{\sigma}}}$ can be solved using standard LP optimization software, e.g, Gurobi [19]. Table 1 presents the basic outline of the algorithm for solving bandgap optimization problems by the linear program (15) instead of the semidefinite program (12). We note in Step 4 of the algorithm that one can augment the solution process for $P_{LP}^{\hat{\boldsymbol{\sigma}}}$ with a standard delayed constraint generation procedure [20]. More detailed implementation of Step 2b is discussed in the next subsection.

TABLE 1. Algorithm for solving bandgap problems using linear inequalities approximation of eigenvalue bounds.

	Algorithm for Bandgap Optimization using Linear Inequalities Approximation
Step 1.	Start with initial guess $\hat{\boldsymbol{\sigma}} := \boldsymbol{\sigma}^0$ and tolerance ε_{tol}
Step 2a.	Construct the matrices for (12) based on $\hat{\boldsymbol{\sigma}}$, for each $\boldsymbol{k} \in \mathscr{P}$, $i = 1, \ldots, n_\sigma$, and $j = 1, \ldots, J$: $A_{ij}^{\hat{\boldsymbol{\sigma}},\ell}(\boldsymbol{k}) := \Phi_j^{\hat{\boldsymbol{\sigma}},\ell *}(\boldsymbol{k}) \mathscr{A}_i(\boldsymbol{k}) \Phi_j^{\hat{\boldsymbol{\sigma}},\ell}(\boldsymbol{k})$, $A_{ij}^{\hat{\boldsymbol{\sigma}},u}(\boldsymbol{k}) := \Phi_j^{\hat{\boldsymbol{\sigma}},u *}(\boldsymbol{k}) \mathscr{A}_i(\boldsymbol{k}) \Phi_j^{\hat{\boldsymbol{\sigma}},u}(\boldsymbol{k})$, $M_{ij}^{\hat{\boldsymbol{\sigma}},\ell}(\boldsymbol{k}) := \Phi_j^{\hat{\boldsymbol{\sigma}},\ell *}(\boldsymbol{k}) \mathscr{M}_i \Phi_j^{\hat{\boldsymbol{\sigma}},\ell}(\boldsymbol{k})$, $M_{ij}^{\hat{\boldsymbol{\sigma}},u}(\boldsymbol{k}) := \Phi_j^{\hat{\boldsymbol{\sigma}},u *}(\boldsymbol{k}) \mathscr{M}_i \Phi_j^{\hat{\boldsymbol{\sigma}},u}(\boldsymbol{k})$.
Step 2b.	Choose approximating vectors $b_{(1)}, \ldots, b_{(N_B)}$ for each of the $2n_k$ SDP inclusions:
Step 2c.	Construct the data for (15) based on $\hat{\boldsymbol{\sigma}}$ and the linear operators from Step 2a: $B_j^{\hat{\boldsymbol{\sigma}},\ell}$, $g_j^{\hat{\boldsymbol{\sigma}},\ell}$, $B_j^{\hat{\boldsymbol{\sigma}},u}$, and $g_j^{\hat{\boldsymbol{\sigma}},u}$
Step 3.	Form the linear problem $P_{LP}^{\hat{\boldsymbol{\sigma}}}$ in (15)
Step 4.	Solve $P_{LP}^{\hat{\boldsymbol{\sigma}}}$ for an optimal solution $(\boldsymbol{\sigma}^*, \boldsymbol{\chi}^{\ell *}, \boldsymbol{\chi}^{u *}, F)$ *(Optional: augment $P_{LP}^{\hat{\boldsymbol{\sigma}}}$ with Delayed Constraint Generation)*
Step 5.	If $\|\boldsymbol{\sigma}^* - \hat{\boldsymbol{\sigma}}\| \leq \varepsilon_{\text{tol}}$, stop. Else update $\hat{\boldsymbol{\sigma}} \leftarrow \boldsymbol{\sigma}^*$ and go to **Step 2.**

4.2 Methodology for Constructing the Approximating Vectors

We describe our approach for constructing the approximating vectors $b_{(1)}, \ldots, b_{(N_B)} \in \mathbb{R}^{N_{sp}}$ for any matrix $B \in \mathbb{R}^{N_{sp} \times N_{sp}}$, e.g., $B := \Phi_j^{\hat{\boldsymbol{\sigma}} *}(\boldsymbol{k}) \mathscr{A}_0(\boldsymbol{k}) \Phi_j^{\hat{\boldsymbol{\sigma}}}(\boldsymbol{k})$. Note that N_{sp}, being the dimension of the approximate and reduced subspace, is not large (recall $N_{sp} \approx 3 - 7$ typically). Ideally, we would want the approximat-

ing vectors to be distributed uniformly over the upper half of the Euclidean sphere: $\{b \in \mathbb{R}^{N_{sp}} : \sqrt{b^T b} = 1,\ b_{N_{sp}} \geq 0\}$, where we need only consider a half-sphere because $v^T M v = (-v)^T M (-v)$ for any $v \in \mathbb{R}^{N_{sp}}$. For ease of construction, we choose to work with the upper half of the unit L_1-sphere, also known as the upper boundary of the cross-polytope $\{b \in \mathbb{R}^{N_{sp}} : \|b\|_1 = 1,\ b_{N_{sp}} \geq 0\}$, whose $2^{(N_{sp}-1)}$ facets are the unit $(N_{sp}-1)$-simplices in their respective orthants. Given an integer dilation constant K, we first define:

$$\mathscr{K} := \left\{ k \in \mathbb{R}^{N_{sp}} : \sum_{i=1}^{N_{sp}} |k_i| = K,\ k_i \text{ integer} \right\}, \qquad (16)$$

and then define the approximating vectors $b_{(1)}, \ldots, b_{(N_B)} \in \mathbb{R}^{N_{sp}}$ to be the elements of the following set:

$$B_K := \left\{ b \in \mathbb{R}^{N_{sp}} : b = (1/K)k \text{ for some } k \in \mathscr{K},\ k_{N_{sp}} \geq 0 \right\}.$$

The resulting approximating vectors are distributed uniformly on the surface of the half cross-polytope. This is illustrated in Figure 1 for $N_{sp} = 2$. Note that the number of vectors in B_K grows as $O(K^{N_{sp}-1})$. Increasing K will render the piecewise linear approximation model more accurate albeit at higher computational cost. In addition and if necessary, we expand the set of approximating vectors at each iteration using *delayed constraint generation*: once the linear optimization problem (15) is solved, we check the semidefinite inclusions in (12) for any eigenvectors violating the constraints and add them to the set of approximating vectors to generate additional linear inequality cuts which are then added to (15). Note that checking the semidefinite inclusions in (12) is inexpensive due to the reduced size of the system.

5 COMPUTATION RESULTS AND DISCUSSION

5.1 Quality of Linear Inequalities Approximation

To verify the quality of the approximation of the semidefinite inclusions by using the linear inequalities, we compare it with the the design of photonic crystals using SDP formulation studied in our earlier work [1]. We focus on the effect of the tunable parameter K (defined in equation (16)) and the resulting number of linear inequalities. We first note that when K is large, more vectors (larger N_B) are generated to presumably approximate semidefinite inclusions more accurately, yielding a linear optimization problem (15) that better approximates the semidefinite problem (12). As a result, the resulting linear optimization problem will contain a larger number of linear inequalities and thus require more computation time. On the other hand, a smaller value of K will reduce the number of linear inequality constraints, but result in a less accurate approximation of (12).

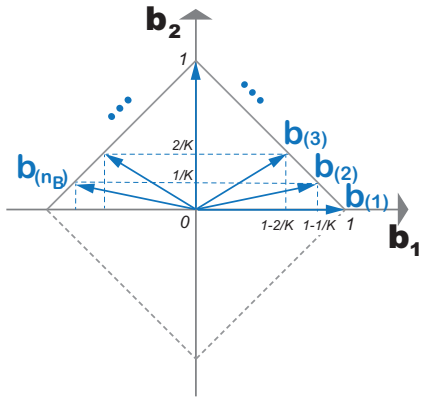

FIGURE 1. The vectors chosen to construct the approximating linear inequalities are distributed uniformly on the surface of a half cross-polytope arising from the L_1 norm.

The quality of the linear inequalities approximation may be empirically measured in terms of the number of outer iterations of the algorithm of Table 1 and the number of "successful" solutions, where a solution is deemed successful if it opens up a bandgap more than 10%.

We conduct an empirical test in order to determine a good value of K. In particular, we make 10 runs of the algorithm of Table 1 using 10 randomly chosen starting point configurations for a variety of types of bandgap problems and report the results in Table 2. In this table, the headings in the right side columns of the form $\Delta_{1,2}^{TE}$ refer to bandgap optimization of the bandgap between the 2nd and 1st eigenvalues in TE polarization, etc. Table 2 shows average outer iterations, and number of successful runs, for various bandgap optimization problems by using the algorithm of Table 1, with a large value of K ($K = 5$, resulting in $N_B \sim 500$) and a small value of K ($K = 3$, resulting in $N_B \sim 10$) combined with delayed constraint generation (DCG). The results of the SDP approach (presented in [1]) are shown in the table as a benchmark for comparison. We observe that using a small value of $K = 3$ combined with delayed constraint generation appears to strike a good compromise between system size (and computation time) and the success rate, and are used in all the subsequent computations.

5.2 Optimal Phononic Bandgap Structures

We present the LP optimization results for the design of phononic crystals made up of two room-temperature solid materials: epoxy and lead. The properties of the softer material epoxy are $\rho_1 = 1180\ \text{kg m}^{-3}$, $C_{T1} = 1160\ \text{m s}^{-1}$, and $C_{L1} = 2540\ \text{m s}^{-1}$, and the properties of the stiffer material lead are $\rho_2 = 11357\ \text{kg m}^{-3}$, $C_{T2} = 860\ \text{m s}^{-1}$, and $C_{L2} = 2158\ \text{m s}^{-1}$

TABLE 2. Average number of outer iterations and the total number of successful runs (out of 10 runs) for bandgap optimization using the semidefinite program (SDP) formulation and the linear program (LP) formulation. $\Delta\lambda_{m,m+1}$ indicates the optimized bandgap is between the mth and the $m+1$st eigenvalues. DCG denotes delayed constraint generation.

	$\Delta\lambda_{1,2}^{TE}$	$\Delta\lambda_{2,3}^{TE}$	$\Delta\lambda_{8,9}^{TE}$	$\Delta\lambda_{9,10}^{TE}$
TE Polarization				
SDP	9.0/*7*	9.0/*6*	14.2/*2*	23.5/*1*
LFP ($K=5$)	17.0/*9*	9.1/*8*	43.5/*3*	40.5/*3*
LFP ($K=3$)	20.0/*6*	12.6/*6*	37.1/*1*	26.1/*2*
LFP ($K=3$) with DCG	14.0/*8*	15.8/*6*	27.7/*3*	24.1/*4*
TM Polarization				
SDP	3.4/*10*	4.1/*8*	10.9/*3*	22.5/*2*
LFP ($K=5$)	5.1/*10*	10.2/*7*	31.2/*3*	36.1/*4*
LFP ($K=3$)	5.2/*10*	6.3/*8*	20.5/*2*	34.2/*2*
LFP ($K=3$) with DCG	5.2/*10*	6.9/*7*	23.2/*2*	27.6/*2*

[16] [1]. We computed a wide range of bandgaps in out-of-plane (OP), in-plane (IP), and coupled out-of-plane and in-plane (IOP) modes for both square and hexagonal lattices. In the results presented herein, the eigenvalues are plotted in the dimensionless unit $\chi a^2/4\pi^2 C_{T1}^2$, where a is the lattice constant for both square and hexagonal lattices.

In order to improve computation efficiency, the mesh adaptivity procedure developed in [12] is also incorporated in all the computations here. With such a procedure, one usually initializes with a very coarse finite element grid (e.g., 8×8 in the square lattice) representing both the field solution and the geometry, and solves to optimality at current resolution before further refining the mesh elements only at the material interface (as dictated by the optimal solution). An interpolated optimal solution of the coarser mesh is then used as the initial solution for the finer mesh. The procedure continues until the mesh is adaptively refined up to a desired resolution (e.g., 128×128).

In all the optimal crystal structures presented in figures 2 to 7, the dark color represents the inclusions made of material lead imbedded in the softer epoxy, which is represented by the white background color. Drawing analogy to the dictum in the photonic crystal bandgap structures "*the TM bandgaps are favored in lattices of isolated high dielectric regions, and TE bandgaps are favored in connected lattices*", we observed one common feature in all the optimal structures here, that is, "*phononic bandgaps are favored in lattices of isolated stiff material*". Further examination reveals that despite the different parameter dependence, the optimal crystal structures for IP propagation (Figures 2 and 3) exhibit astonishing similar topology to the optimal photonic crystal structures for TM polarization. Nevertheless, no interesting resemblance is observed in the more complicated IP and IOP propagation modes.

[1] C_T and C_L are the velocities at which transverse and longitudinal elastic waves propagate. The mechanical properties – the Lamè parameters of the underlying solid material can be computed from the formulas,

$$\mu = \rho C_T^2, \quad \lambda = \rho(C_L^2 - 2C_T^2).$$

6 CONCLUSION

Motivated by our new modeling paradigm "fabrication-adaptive optimization" [14], a linear program (LP) based algorithm is proposed in this work to solve the bandgap optimization problems for phononic crystals. The LP formulation is then compared to the SDP formulation [1] to demonstrate its approximation quality and improved efficiency. The proposed algorithm is shown to be able to solve a variety of phononic crystal design problems of different propagation modes and different lattice structures.

The successful application of the LP formulation in both types of microstructured materials (photonic and phononic) design not only suggests its further applicability to a broad category of eigenvalue-driven optimization problems, but also enables us to extend the development of fabrication-adaptive optimizations to other engineering design problems.

ACKNOWLEDGMENT

This work is supported by AFOSR Grant No. FA9550-11-1-0141, the Singapore-MIT Alliance, the MIT- Chile-Pontificia Universidad Catlica de Chile Seed Fund, and LaCaixa Fellowship.

REFERENCES

[1] Men, H., Nguyen, N., Freund, R., Parrilo, P., and Peraire, J., 2010. "Bandgap optimization of two-dimensional photonic crystals using semidefinite programming and subspace methods". *Journal of Computational Physics,* ***229***, pp. 3706–3725.

[2] Kushwaha, M., Halevi, P., Dobrzynski, L., and Djafari-Rouhani, B., 1993. "Acoustic band structure of periodic elastic composites". *Physical Review Letters,* ***71***(13), pp. 2022–2025.

[3] Khelif, A., Choujaa, A., Djafari-Rouhani, B., Wilm, M., Ballandras, S., and Laude, V., 2003. "Trapping and guiding of acoustic waves by defect modes in a full-band-gap ultrasonic crystal". *physical Review B,* ***68***(21), p. 214301.

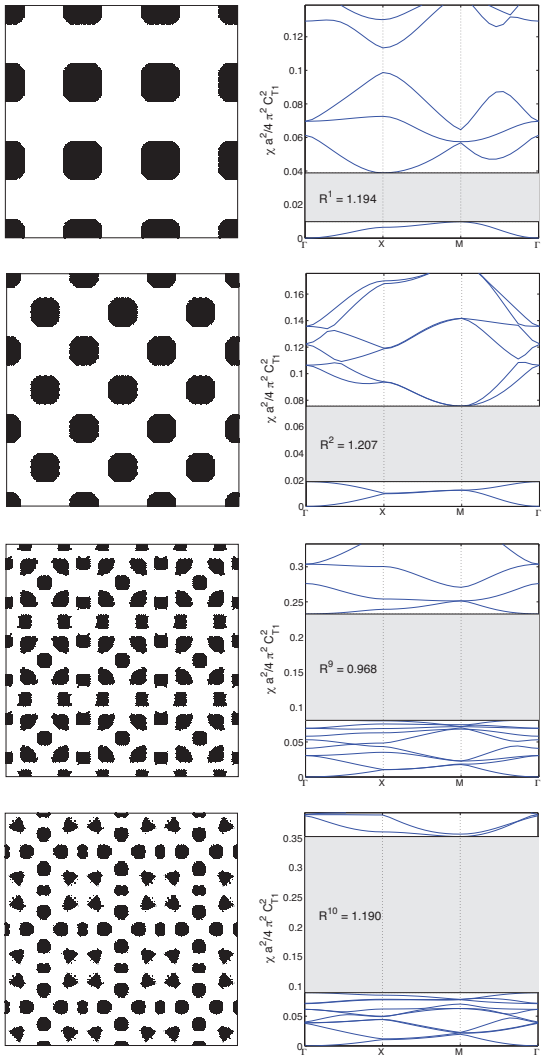

FIGURE 2. Optimization of various OP bandgaps in square lattice. Left column shows the optimal crystal structures, and the plots in the right column are the corresponding eigenfrequency structures.

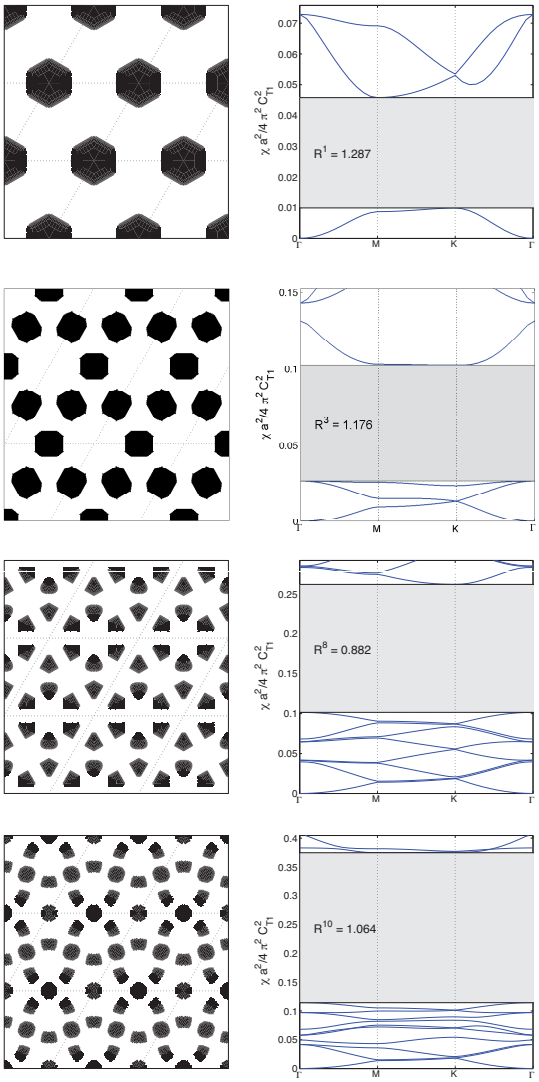

FIGURE 3. Optimization of various OP bandgaps in hexagonal lattice. Left column shows the optimal crystal structures, and the plots in the right column are the corresponding eigenfrequency structures.

[4] Khelif, A., Choujaa, A., Benchabane, S., Djafari-Rouhani, B., and Laude, V., 2004. "Guiding and bending of acoustic waves in highly confined phononic crystal waveguides". *Applied Physics Letters,* ***84***(22), pp. 4400–4402.

[5] Sigmund, O., Jensen, S., et al., 2003. "Systematic design of phononic band–gap materials and structures by topology optimization". *Philosophical Transactions A,* ***361***(1806), p. 1001.

[6] Bilal, O. R., and Hussein, M. I., 2011. "Ultrawide phononic band gap for combined in-plane and out-of-plane waves". *Physical Review E,* ***84***(6), p. 065701.

[7] Halkjær, S., Sigmund, O., and Jensen, J. S., 2005. "Inverse design of phononic crystals by topology optimization". *Zeitschrift für Kristallographie,* ***220***(9-10), pp. 895–905.

[8] Halkjær, S., Sigmund, O., and Jensen, J. S., 2006. "Maximizing band gaps in plate structures". *Structural and Multidisciplinary Optimization,* ***32***(4), pp. 263–275.

[9] Sigmund, O., 2009. "Systematic design of metamaterials by topology optimization". In IUTAM Symposium

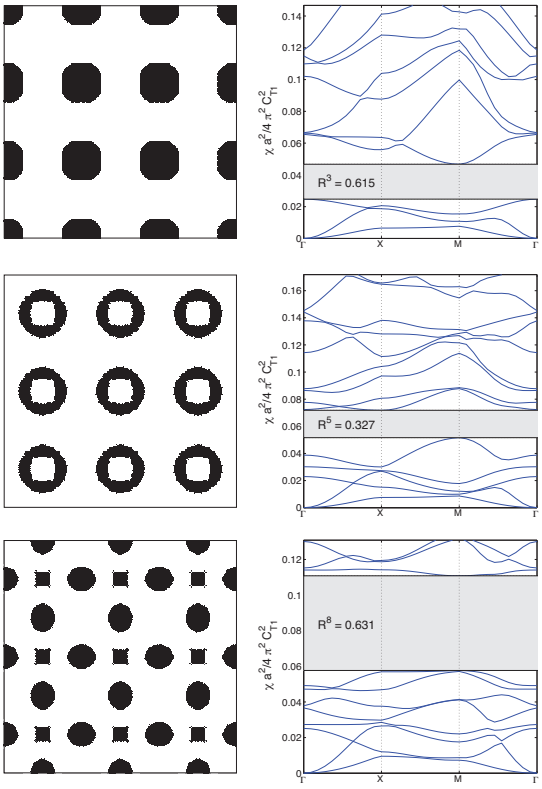

FIGURE 4. Optimization of various IP bandgaps in square lattice. Left column shows the optimal crystal structures, and the plots in the right column are the corresponding eigenfrequency structures.

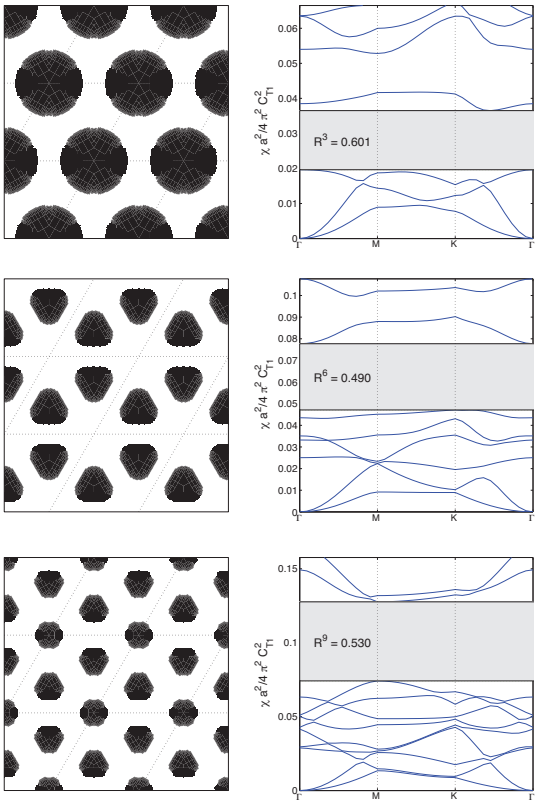

FIGURE 5. Optimization of various IP bandgaps in hexagonal lattice. Left column shows the optimal crystal structures, and the plots in the right column are the corresponding eigenfrequency structures.

on Modelling Nanomaterials and Nanosystems, Springer, pp. 151–159.

[10] Langlet, P., Hladky-Hennion, A.-C., and Decarpigny, J.-N., 1995. "Analysis of the propagation of plane acoustic waves in passive periodic materials using the finite element method". *The Journal of the Acoustical Society of America,* ***98***, p. 2792.

[11] Svanberg, K., 1987. "The method of moving asymptotesa new method for structural optimization". *International journal for numerical methods in engineering,* ***24***(2), pp. 359–373.

[12] Men, H., Nguyen, N., Freund, R., Lim, K., Parrilo, P., and Peraire, J., 2011. "Design of photonic crystals with multiple and combined band gaps". *Physical Review E,* ***83***(4), p. 046703.

[13] Kao, C. Y., Osher, S., and Yablonovitch, E., 2005. "Maximizing band gaps in two-dimensional photonic crystals by using level set methods". *Applied Physics B: Lasers and Optics,* ***81***(2), pp. 235–244.

[14] Men, H., Nguyen, N., Saa-Seoane, J., Freund, R., and Peraire, J., 2012. "Fabrication-adaptive optimization, with an application to photonic crystal design". *Submitted*.

[15] Lewis, A., 2002. Robust regularization. Technical report, Simon Fraser University.

[16] Maldovan, M., and Thomas, E., 2008. *Periodic Materials and Interference Lithography for Photonics, Phononics and Mechanics*. Wiley-VCH.

[17] Charnes, A., and Cooper, W. W., 1962. "Programming with linear functionals". *Naval Research Logistics Quarterly,* ***9***.

[18] Tütüncü, R. H., Toh, K. C., and Todd, M. J., 2003. "Solving semidefinite-quadratic-linear programs using SDPT3". *Mathematical Programming,* ***95***(2), pp. 189–217.

[19] Gurobi Optimization, I., 2012. Gurobi optimizer reference manual.

[20] Bertsimas, D., and Tsitsiklis, J., 1997. *Introduction to Linear Optimization*. Athena Scientific.

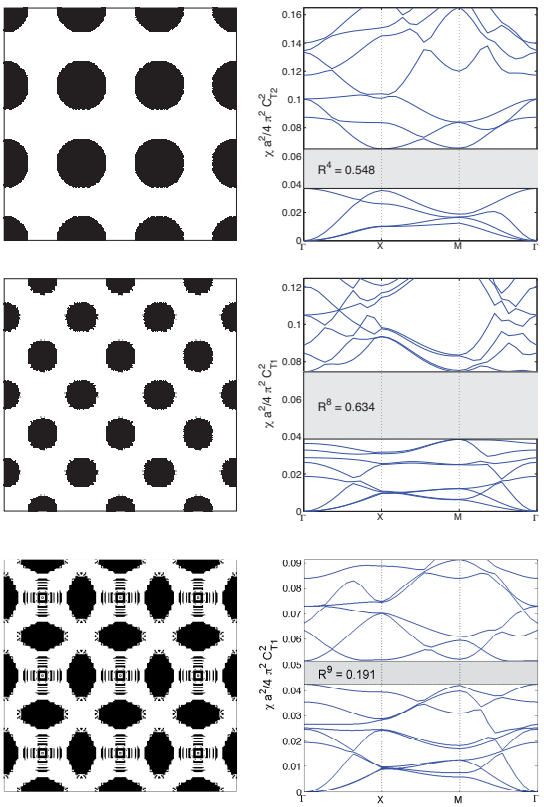

FIGURE 6. Optimization of various IOP bandgaps in square lattice. Left column shows the optimal crystal structures, and the plots in the right column are the corresponding eigenfrequency structures.

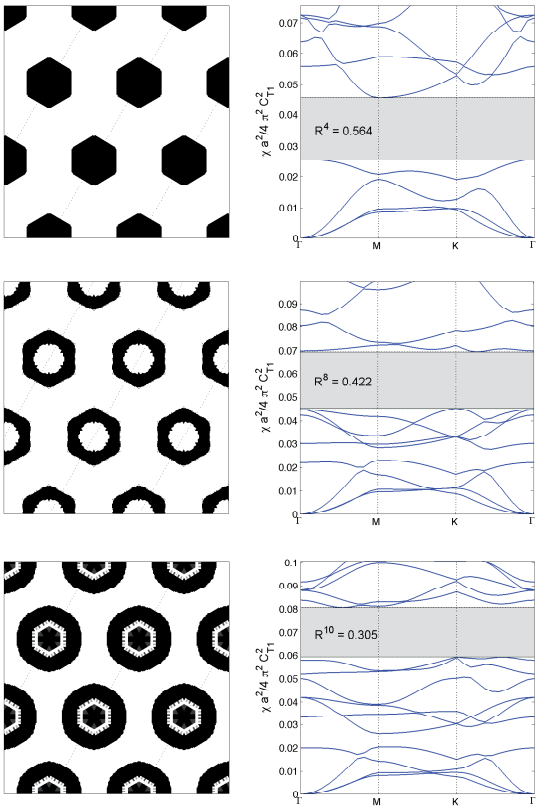

FIGURE 7. Optimization of various IOP bandgaps in hexagonal lattice. Left column shows the optimal crystal structures, and the plots in the right column are the corresponding eigenfrequency structures.